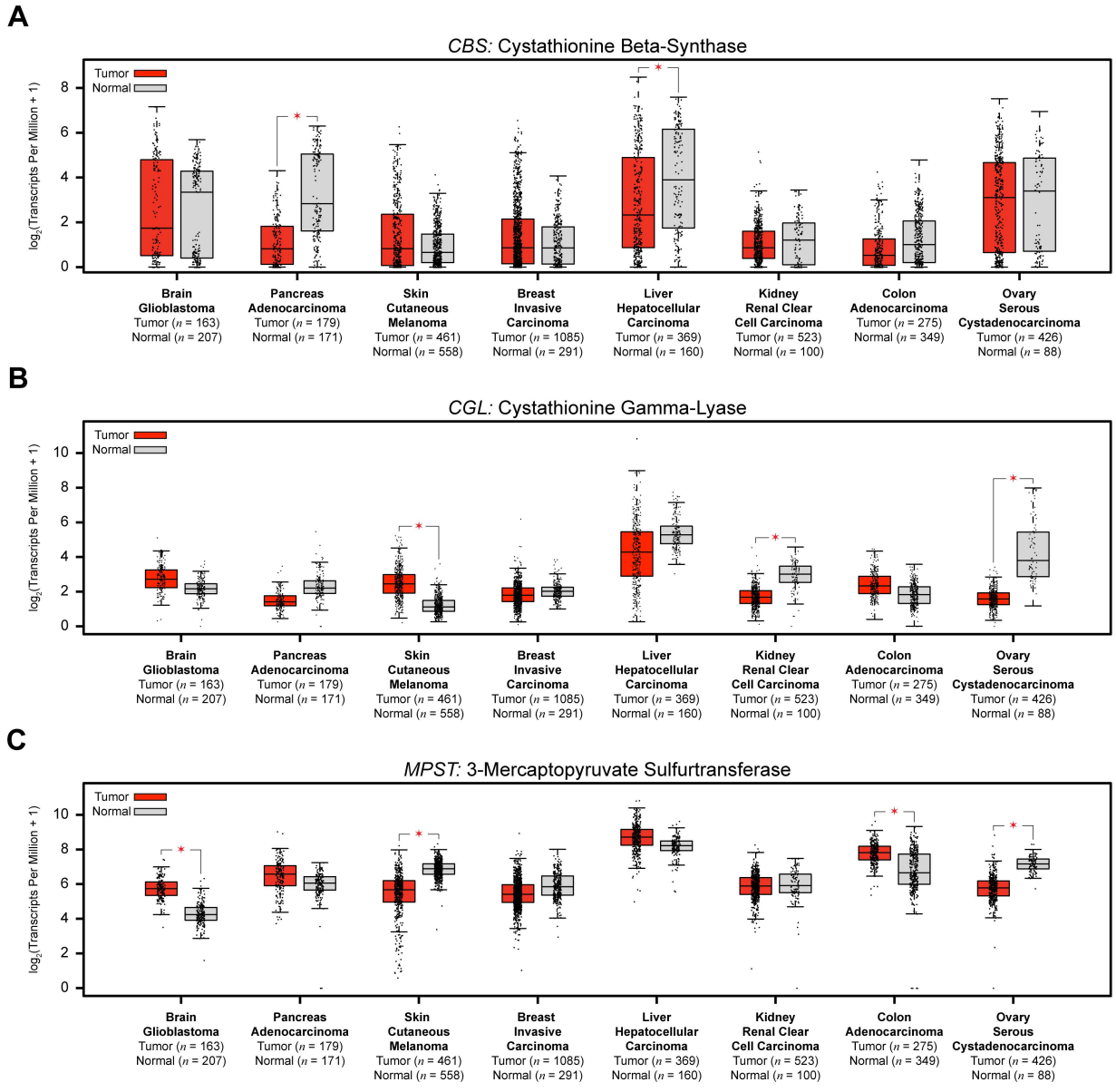
A
CBS: Cystathionine Beta-Synthase
B
CGL: Cystathionine Gamma-Lyase
C
MPST: 3-Mercaptopyruvate Sulfurtransferase
Tumor
Normal
log2(Transcripts Per Million + 1)
Brain Glioblastoma Tumor (n = 163) Normal (n = 207)
Pancreas Adenocarcinoma Tumor (n = 179) Normal (n = 171)
Skin Cutaneous Melanoma Tumor (n = 461) Normal (n = 558)
Breast Invasive Carcinoma Tumor (n = 1085) Normal (n = 291)
Liver Hepatocellular Carcinoma Tumor (n = 369) Normal (n = 160)
Kidney Renal Clear Cell Carcinoma Tumor (n = 523) Normal (n = 100)
Colon Adenocarcinoma Tumor (n = 275) Normal (n = 349)
Ovary Serous Cystadenocarcinoma Tumor (n = 426) Normal (n = 88)

Supplementary Figure 1. *mRNA Expression Data Comparing Normal to Neoplastic Tissues Confirms Heterogeneous and Organ Specific Expression of the H_2S Synthesizing Enzymes*. (A) CBS, (B) CGL, and (C) MPST. Data was curated and downloaded from the GEPIA dataset. The following solid organs and associated tumors were analyzed: (1) Normal brain *versus* GBM. (2) Normal pancreas *versus* pancreatic adenocarcinoma. (3) Normal skin *versus* cutaneous melanoma. (4) Normal breast *versus* invasive breast carcinoma. (5) Normal liver *versus* hepatocellular carcinoma. (6) Normal kidney *versus* clear cell renal carcinoma. (7) Normal colon *versus* colon adenocarcinoma. (8) Normal ovary *versus* serous ovarian cystic adenocarcinoma. Gene expression in the neoplastic state is designated in red as compared to the physiologically normal state, represented in gray. Statistically significant ($p \leq 0.05$) differences in average gene expression were designated with red asterisks.

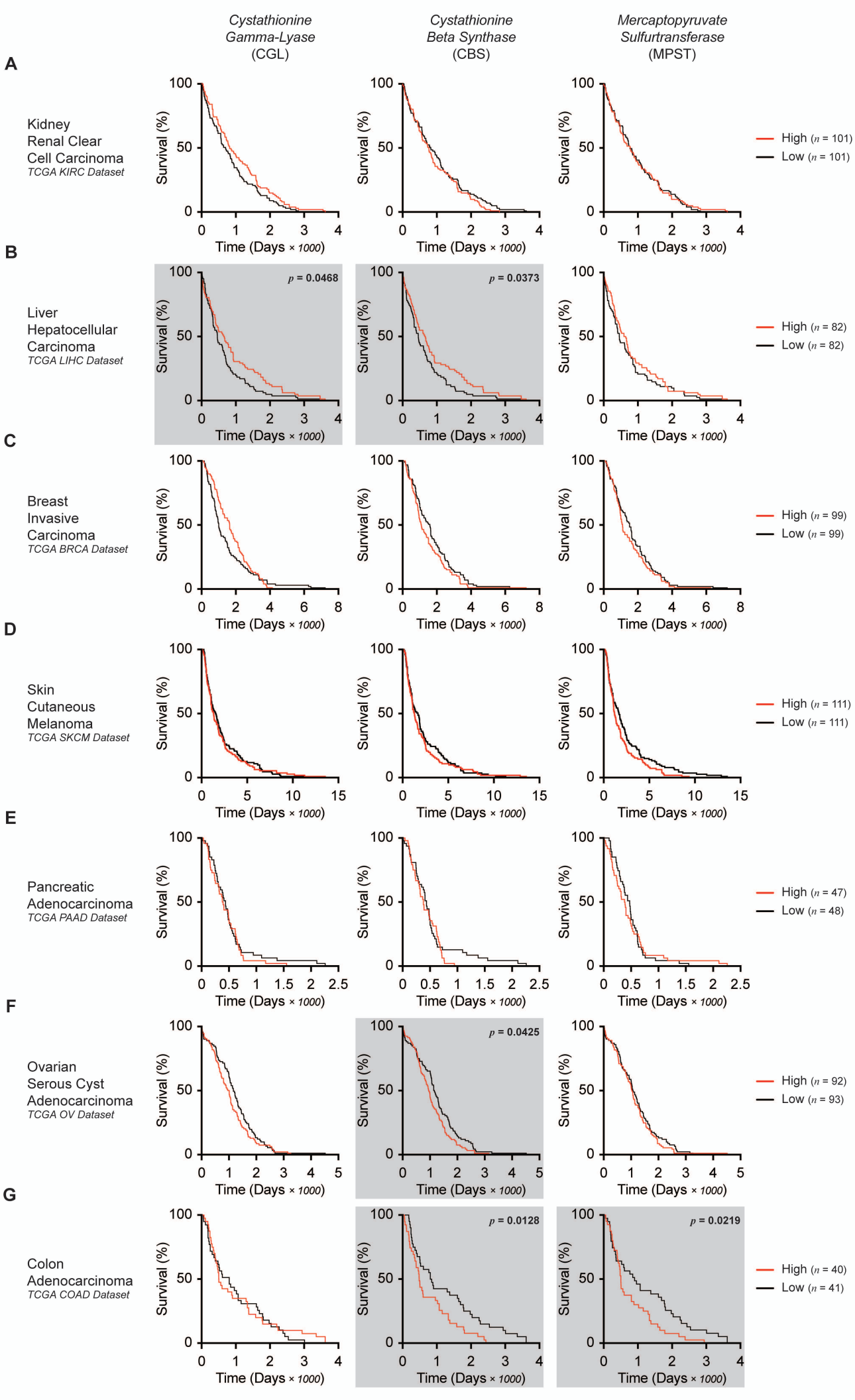
Cystathionine Gamma-Lyase (CGL)
Cystathionine Beta Synthase (CBS)
Mercaptopyruvate Sulfurtransferase (MPST)
A
Kidney Renal Clear Cell Carcinoma
TCGA KIRC Dataset
B
Liver Hepatocellular Carcinoma
TCGA LIHC Dataset
p = 0.0468
p = 0.0373
C
Breast Invasive Carcinoma
TCGA BRCA Dataset
D
Skin Cutaneous Melanoma
TCGA SKCM Dataset
E
Pancreatic Adenocarcinoma
TCGA PAAD Dataset
F
Ovarian Serous Cyst Adenocarcinoma
TCGA OV Dataset
p = 0.0425
G
Colon Adenocarcinoma
TCGA COAD Dataset
p = 0.0128
p = 0.0219
Survival (%)
Time (Days × 1000)
High (n = 101)
Low (n = 101)
High (n = 82)
Low (n = 82)
High (n = 99)
Low (n = 99)
High (n = 111)
Low (n = 111)
High (n = 47)
Low (n = 48)
High (n = 92)
Low (n = 93)
High (n = 40)
Low (n = 41)

Supplemental Figure 2. *Kaplan-Meier Analysis of H_2S-Synthesizing Enzymes in the Contexts of Multiple Solid Tissue Cancers.* The University of California Santa Cruz Genome Browser was used to filter, download, and analyze mRNA expression data correlated to patient survival for the following solid tissue cancers and associated datasets: (1) Renal clear cell adenocarcinoma; *KIRC Dataset*. (2) Hepatocellular carcinoma; *LIHC Dataset*. (3) Invasive breast carcinoma; *BRCA Dataset*. (4) Cutaneous melanoma; *SKCM Dataset*. (5) Pancreatic adenocarcinoma; *PAAD Dataset*. (6) Ovarian serous cystic adenocarcinoma; *OV Dataset*. (7) Colon adenocarcinoma; *COAD Dataset*. Median gene expression was used to differentiate between high and low expressing patients. Statistically significant ($p \leq 0.05$) results in which enzyme expression predicted patient survival are highlighted in gray.

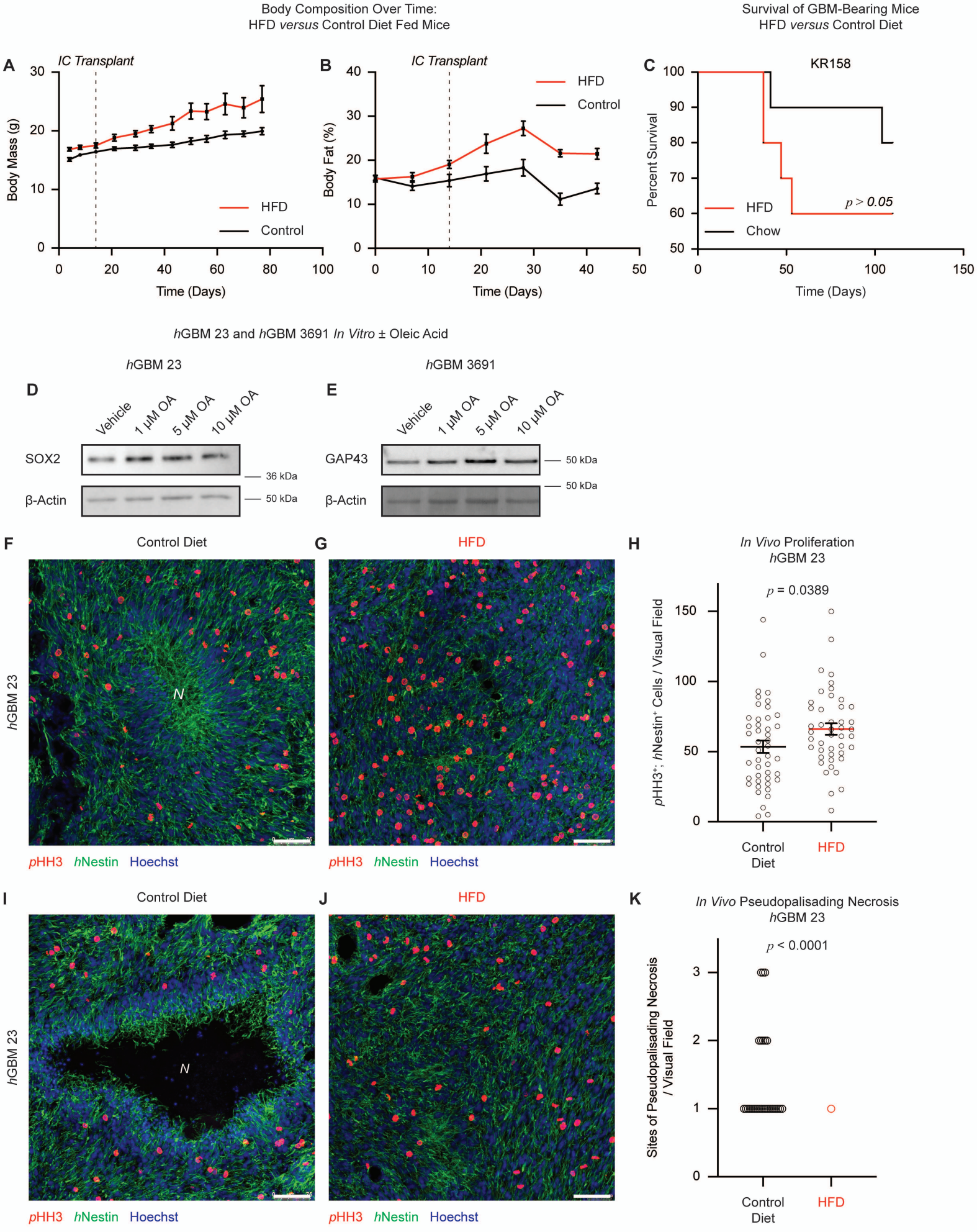
Body Composition Over Time:
HFD versus Control Diet Fed Mice
Survival of GBM-Bearing Mice
HFD versus Control Diet
A
IC Transplant
Body Mass (g)
Time (Days)
HFD
Control
B
IC Transplant
Body Fat (%)
Time (Days)
HFD
Control
C
KR158
Percent Survival
Time (Days)
HFD
Chow
p > 0.05
hGBM 23 and hGBM 3691 In Vitro ± Oleic Acid
hGBM 23
hGBM 3691
D
E
Vehicle
1 μM OA
5 μM OA
10 μM OA
SOX2
β-Actin
36 kDa
50 kDa
GAP43
β-Actin
50 kDa
50 kDa
F
Control Diet
G
HFD
hGBM 23
N
pHH3 hNestin Hoechst
H
In Vivo Proliferation
hGBM 23
p = 0.0389
pHH3+; hNestin+ Cells / Visual Field
Control Diet
HFD
I
Control Diet
J
HFD
hGBM 23
N
pHH3 hNestin Hoechst
K
In Vivo Pseudopalisading Necrosis
hGBM 23
p < 0.0001
Sites of Pseudopalisading Necrosis / Visual Field
Control Diet
HFD

Supplementary Figure 3. *Obesogenic HFD Consumption Leads to Expansion of Treatment-Refractory CSCs, Increased Tumor Cell Proliferation, Protection from Necrotic Cell Death, and Truncated Overall Survival.* (**A, B**) Representative assessments of body mass and fat compositional changes over time as a function of HFD *versus* control diet consumption. Each in vivo experiment was tracked using these metrics beginning from the introduction of the differential diets throughout the post-transplantation period. (**C**) For any cell dosage, Kaplan-Meier survival analysis of the syngeneic GBM model KR158 demonstrated the expected pattern of HFD-mediated disease acceleration; however, statistical testing was confounded based on imperfect disease penetrance. Protein analysis of cultured, patient-derived GBM models demonstrates increased CSC-associated protein expression resulting from exposure to high-fat conditions. In two separate human GBM cellular models (*h*GBM 23 and *h*GBM 3691), administration of oleic acid resulted in dose-responsive expression increases of (**D**) SOX2 and (**E**) GAP43, respectively, compared to vehicle control conditions. In both cases, maximal CSC marker expression resulted from treatment with 5 μM oleic acid. Representative experiments from three biological replicates are presented. Comparative immunofluorescence analysis of the GBM tumor microenvironment confirms increased tumor cell proliferation in the context of HFD consumption compared to consumption of a control diet (**F – H**). Further, sites of pseudopalisading necrosis were more prevalent in animals fed the control diet compared to those fed the HFD (**F** and **I – K**). From 45 images, captured from 3 animals per diet, one necrotic site was identified within the HFD group, whereas 39 sites were identified under control conditions. Mitotic tumor cells were visualized using phospho-histone H3 (*p*HH3, red) multiplexed with human-specific nestin (*h*Nestin, green). Nuclei were visualized with Hoechst (blue). Scale bar = 75 μm. *N* designates sites of pseudopalisading necrosis.

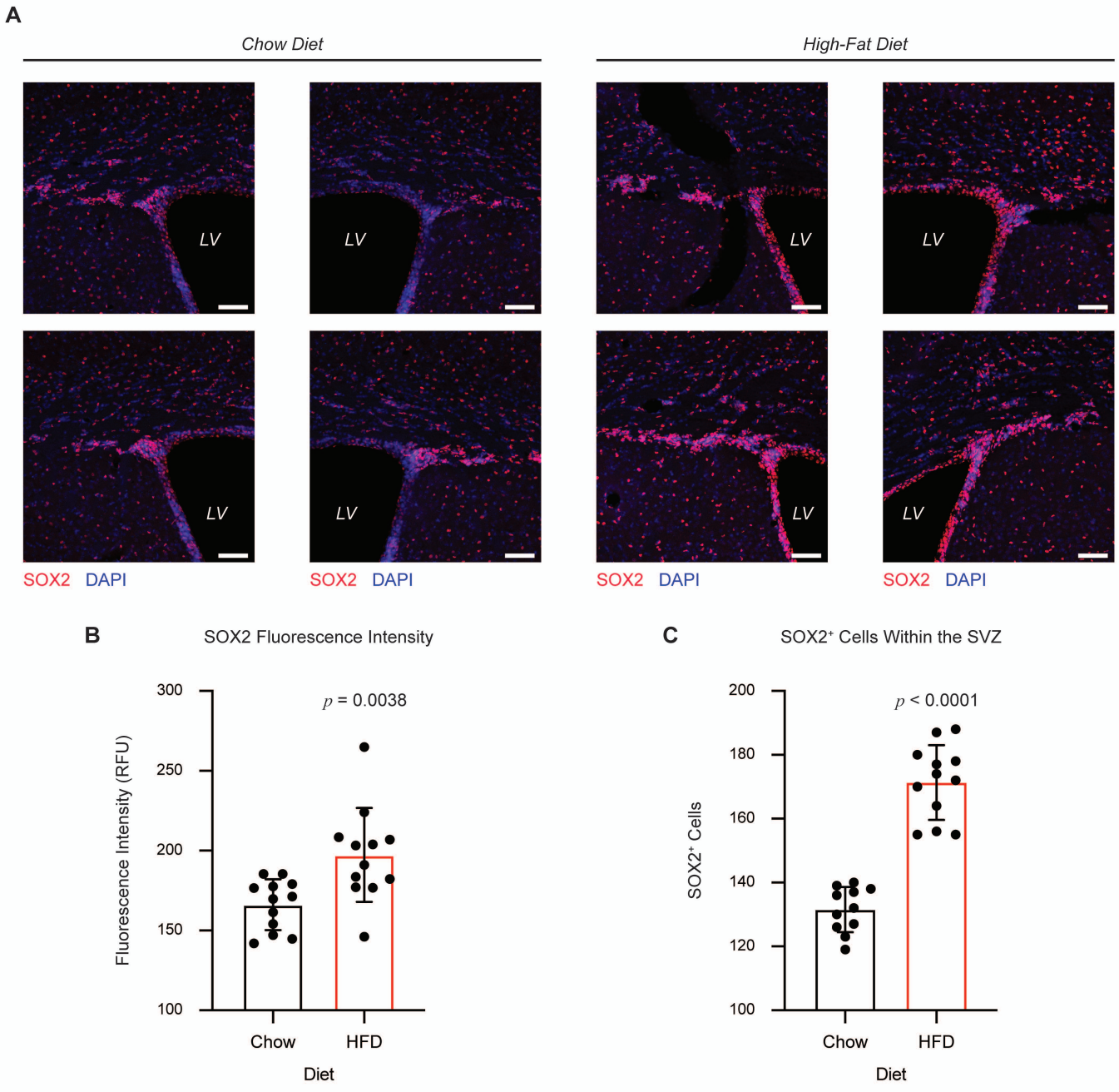
A
Chow Diet
High-Fat Diet
LV
SOX2 DAPI
B
SOX2 Fluorescence Intensity
p = 0.0038
Fluorescence Intensity (RFU)
300
250
200
150
100
Chow
HFD
Diet
C
SOX2⁺ Cells Within the SVZ
p < 0.0001
SOX2⁺ Cells
200
180
160
140
120
100
Chow
HFD
Diet

Supplementary Figure 4. *The HFD-Fed Brain Fosters Expansion of the Neural Stem and Progenitor Cell Pool within the Subventricular Zone.* (**A**) Representative bilateral immunofluorescent micrographs of the subventricular germinal zone of HFD- *versus* chow-fed mice. The neural stem cell-associated transcription factor SOX2 was visualized in red, and nuclei were visualized in blue using DAPI. A total of 12 representative images were captured from a total of 3 animals per group. Quantification based on (**B**) SOX2 fluorescence intensity or (**C**) direct counting of nucleated $SOX2^{+}$ cells confirmed expansion of the NSPC population under HFD-fed conditions compared to control diet. p values determined by unpaired t-test.

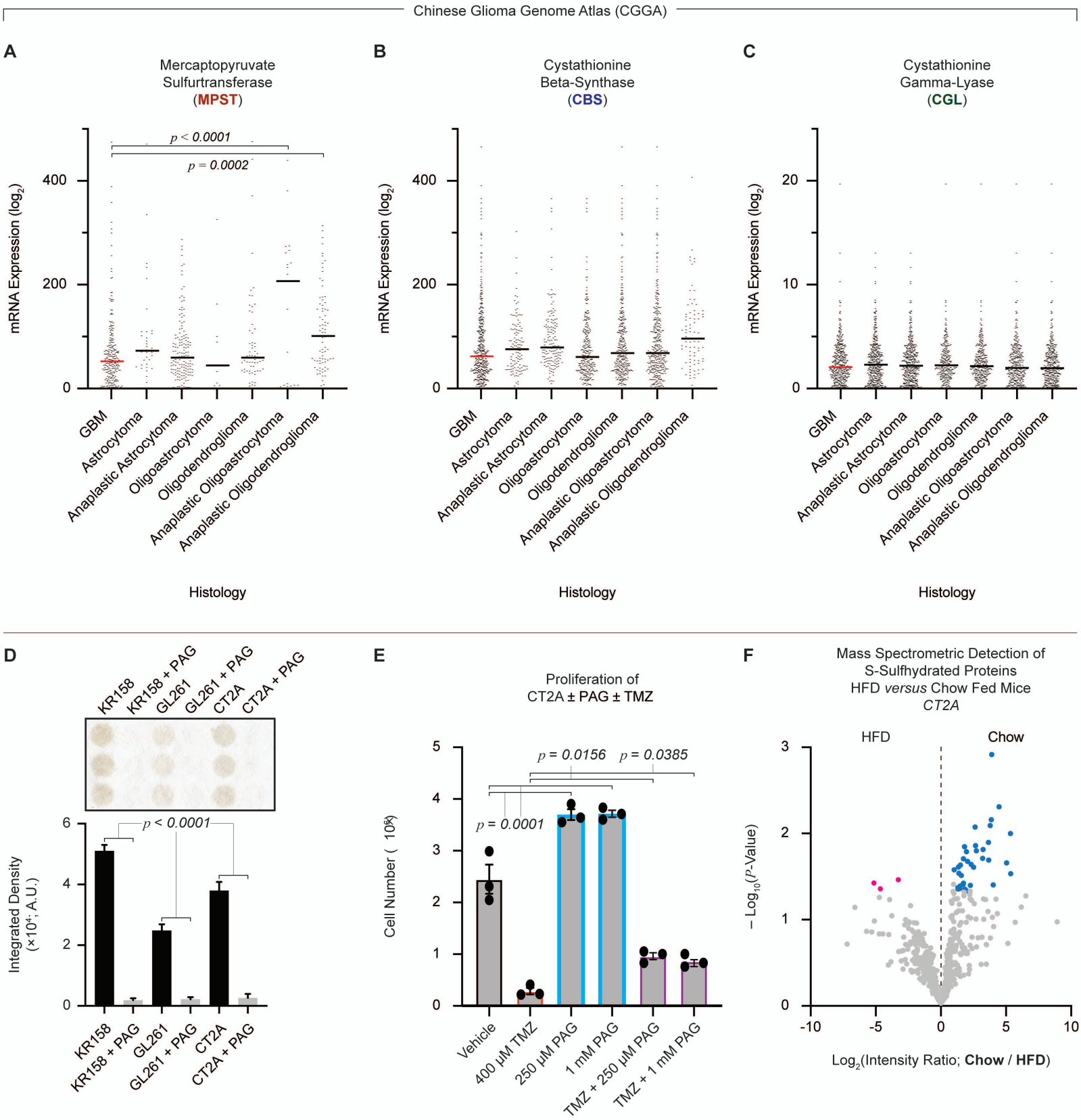
Chinese Glioma Genome Atlas (CGGA)
A
Mercaptopyruvate Sulfurtransferase (MPST)
p < 0.0001
p = 0.0002
mRNA Expression (log2)
GBM
Astrocytoma
Anaplastic Astrocytoma
Oligoastrocytoma
Oligodendroglioma
Anaplastic Oligoastrocytoma
Anaplastic Oligodendroglioma
Histology
B
Cystathionine Beta-Synthase (CBS)
C
Cystathionine Gamma-Lyase (CGL)
D
KR158
KR158 + PAG
GL261
GL261 + PAG
CT2A
CT2A + PAG
p < 0.0001
Integrated Density (×10⁴; A.U.)
E
Proliferation of CT2A ± PAG ± TMZ
p = 0.0156
p = 0.0385
p = 0.0001
Cell Number (10⁶)
Vehicle
400 μM TMZ
250 μM PAG
1 mM PAG
TMZ + 250 μM PAG
TMZ + 1 mM PAG
F
Mass Spectrometric Detection of S-Sulfhydrated Proteins HFD versus Chow Fed Mice CT2A
HFD
Chow
− Log10(P-Value)
Log2(Intensity Ratio; Chow / HFD)

Supplementary Figure 5. *Inhibition of H_2S Synthesis Drives Tumor Cell Proliferation and Chemotherapy Resistance.* (**A – C**) mRNA expression data curated by The CGGA of the three H_2S-synthesizing enzymes, MPST, CBS, and CGL, demonstrate that patients with GBM present the lowest average expression of MPST and CBS compared to patients with other tumor types within the glioma family. (**D**) In vitro verification that the CGL inhibitor PAG effectively attenuates H_2S production from the syngeneic GBM models KR158, GL261, and CT2A. Each well contains lysate from separate biological replicates. For a given cellular model, the p value was determined using an unpaired t-test. (**E**) Direct cell counting verifies that H_2S inhibition increases tumor cell proliferation and resistance to the standard-of-care chemotherapeutic temozolomide (TMZ). Data represent mean ± SEM. p value determined using one-way ANOVA and Tukey's multiple comparison test. (**F**) Volcano plot representing the global analysis of the S-sulfhydrated protein landscape in CT2A tumor-bearing mice fed *either* a HFD *or* a control chow diet.

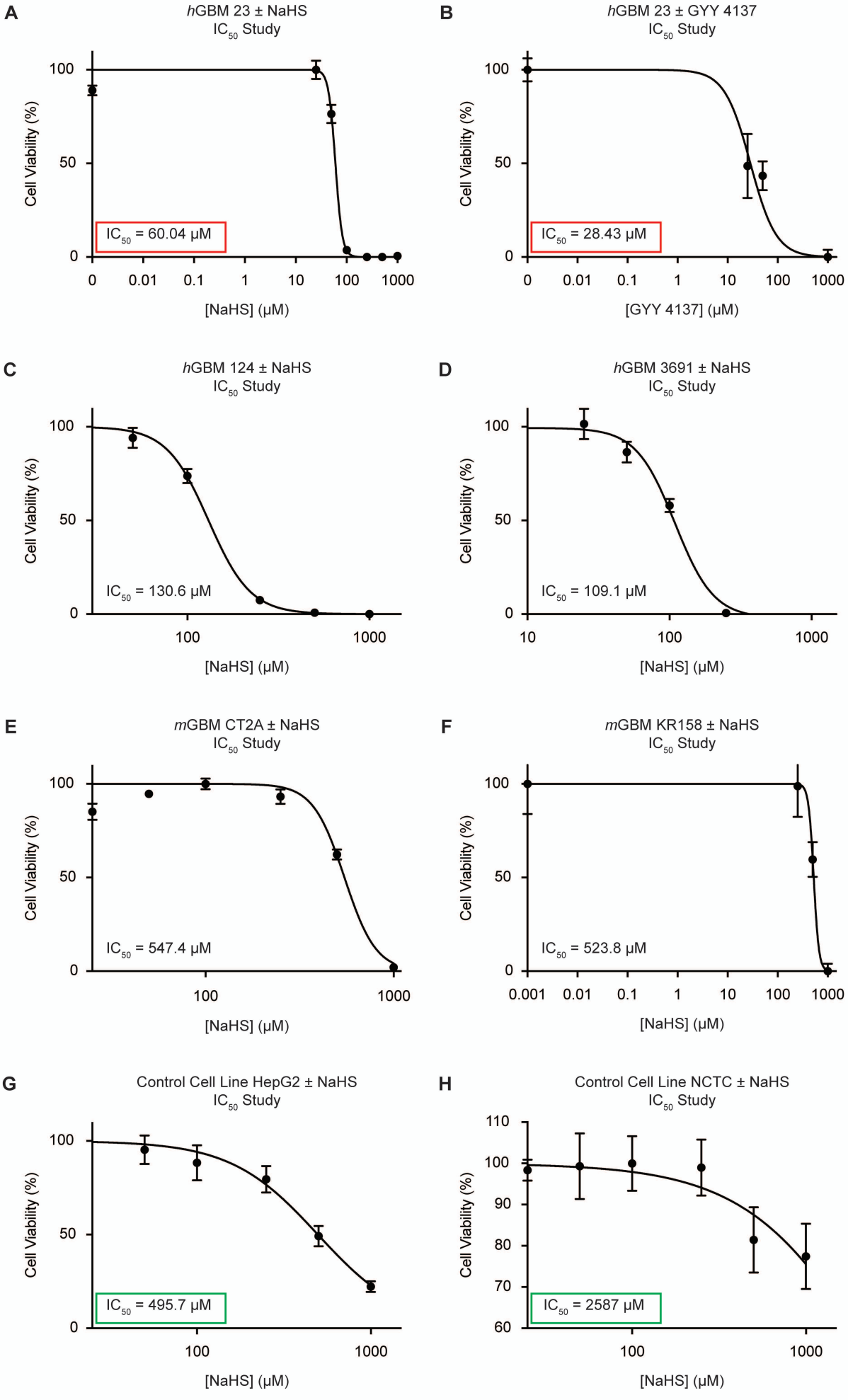
A
hGBM 23 ± NaHS
IC50 Study
Cell Viability (%)
IC50 = 60.04 μM
[NaHS] (μM)
B
hGBM 23 ± GYY 4137
IC50 Study
Cell Viability (%)
IC50 = 28.43 μM
[GYY 4137] (μM)
C
hGBM 124 ± NaHS
IC50 Study
Cell Viability (%)
IC50 = 130.6 μM
[NaHS] (μM)
D
hGBM 3691 ± NaHS
IC50 Study
Cell Viability (%)
IC50 = 109.1 μM
[NaHS] (μM)
E
mGBM CT2A ± NaHS
IC50 Study
Cell Viability (%)
IC50 = 547.4 μM
[NaHS] (μM)
F
mGBM KR158 ± NaHS
IC50 Study
Cell Viability (%)
IC50 = 523.8 μM
[NaHS] (μM)
G
Control Cell Line HepG2 ± NaHS
IC50 Study
Cell Viability (%)
IC50 = 495.7 μM
[NaHS] (μM)
H
Control Cell Line NCTC ± NaHS
IC50 Study
Cell Viability (%)
IC50 = 2587 μM
[NaHS] (μM)

Supplementary Figure 6. *In Vitro Treatment with Exogeneous H_2S Leads to Decreased Viability of GBM Tumor Cells*. Viability in the context of the chemical H_2S donors NaHS and GYY 4137 was tested using the CellTiter-Glo Luminescent Cell Viability Assay. Luminescence was measured after 3 days of treatment with the following concentrations of H_2S donors supplemented into normal growth media: 0.001 μM, 25 μM, 50 μM, 100 μM, 250 μM, 500 μM, and 1000 μM. Five technical replicates were examined per concentration, and each experiment was repeated in triplicate. We observed a stark division in IC_{50} values between the human GBM models (**A – D**) (*h*GBM 23, *h*GBM 124, and *h*GBM 3691), the syngeneic GBM models (**E, F**) (CT2A and KR158) and the control epithelial cancer lines (**G, H**) (HepG2 and NCTC 1469).

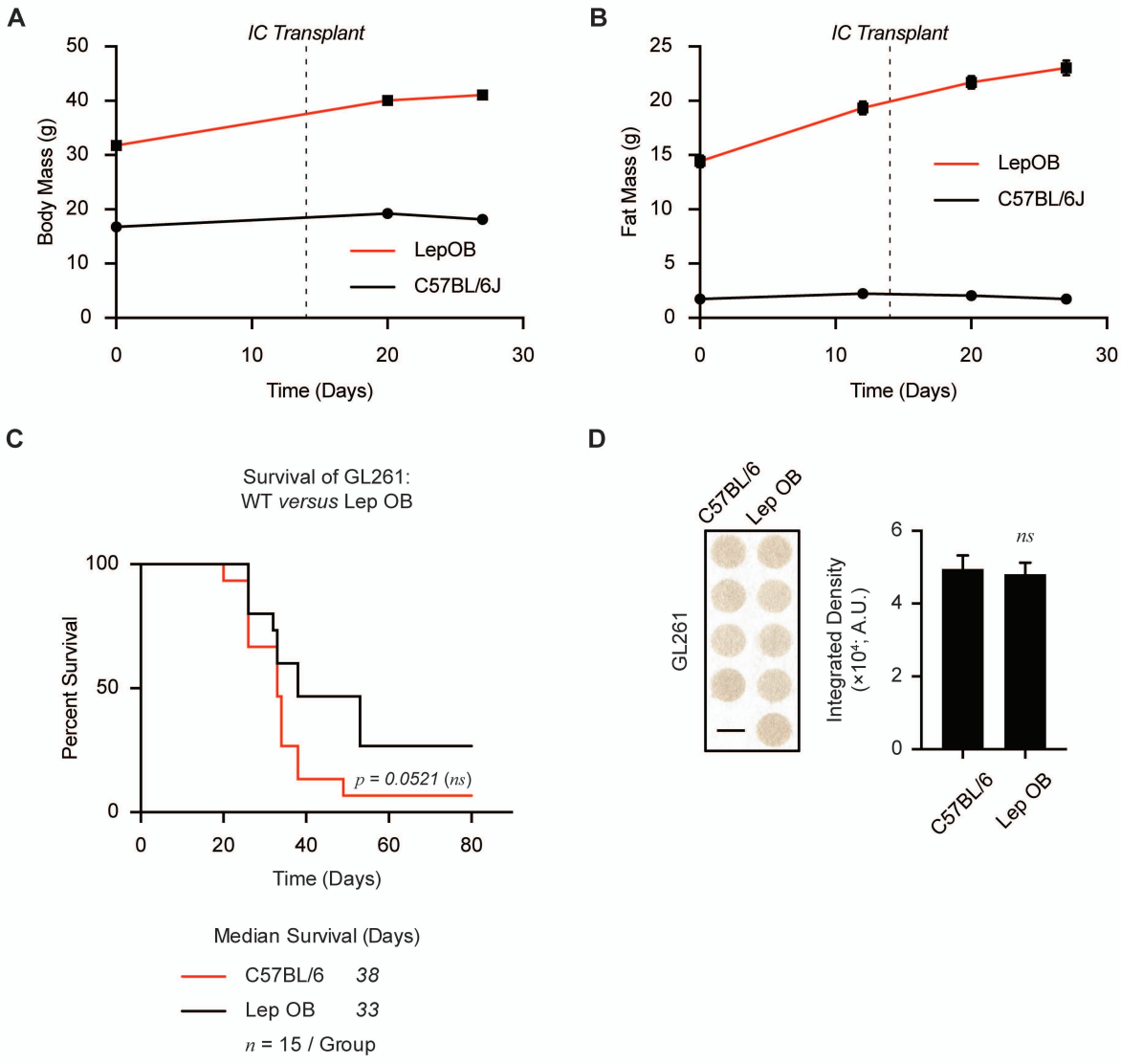
A
IC Transplant
Body Mass (g)
50
40
30
20
10
0
0
10
20
30
Time (Days)
LepOB
C57BL/6J
B
IC Transplant
Fat Mass (g)
25
20
15
10
5
0
0
10
20
30
Time (Days)
LepOB
C57BL/6J
C
Survival of GL261:
WT versus Lep OB
Percent Survival
100
50
0
0
20
40
60
80
Time (Days)
p = 0.0521 (ns)
Median Survival (Days)
C57BL/6 38
Lep OB 33
n = 15 / Group
D
C57BL/6
Lep OB
GL261
Integrated Density
(×10⁴; A.U.)
6
4
2
0
ns
C57BL/6
Lep OB

Supplementary Figure 7. *HFD Consumption Rather than Genetic Obesity Accelerates GBM and Attenuates H_2S Synthesis.* (**A, B**) Representative assessments of body mass and fat compositional changes over time in the context of leptin knockout *versus* wild-type C57BL/6J genetics. (**C**) Kaplan-Meier survival analysis indicates that overall survival between GBM-bearing C57BL/6J and genetically obese LepOB mice was mathematically indistinguishable as determined by log-rank statistical analysis. Additionally, (**D**) intracerebral H_2S synthesis remained intact in the context of genetic leptin knockout. Each well contains brain and tumor tissue homogenate from separate and distinct experimental animals. *p* values determined by unpaired t-test.